Automated Characterization of Autism Spectrum Disorder using Combined Functional and Structural MRI Analysis

Nour El Houda Mezrioui[1], Kamel Aloui[2], Amine Nait-Ali[3], Mohamed Saber Naceur[4]
LTSIRS-LR20ES06, National Engineering School of Carthage, Ariana, Tunisia[1]
LTSIRS-LR20ES06, National Engineering School of Tunisia Sousse, Tunisia[2]
LISSI, Université Paris-Est Créteil Paris, France[3]
LTSIRS-LR20ES06, INSAT-UCAR, Ariana, Tunisia[4]

***Abstract*—Autism Spectrum Disorders (ASD) are among the most critical health concerns of our time. These disorders typically present challenges in social interaction, communication, and exhibit repetitive behaviors. To diagnose and customize medical treatments for ASD effectively, the development of robust neuroimaging biomarkers is indispensable. Although extensive studies have recently delved into this area, only a handful have explored the differences between ASD and NC. This study aspires to shed light on this relationship by analyzing both structural and functional brain data associated with ASD. We aim to provide an extensive characterization of ASD by combining techniques of structural and functional analysis. The framework we propose is based on analyzing the differences in structural and functional aspects between ASD and development control (DC) subjects. The study leverages a substantial dataset of 1114 T1-weighted structural and functional Magnetic Resonance Imaging comprising 521 individuals with ASD and 593 controls, ranging in age from 5 to 64 years. These subjects are divided into three broad age categories. Utilizing automated labeling, we compute the features from subcortical and cortical regions. Statistical analyses help identify disparities between ASD and DC subjects. Principal Component Analysis (PCA) is employed to select the most discriminative features, which are subsequently used for classifying the two groups via an Artificial Neural Network (ANN) analysis. Our preliminary findings reveal a significant difference in the distribution of all tested features and subcortical regions between ASD subjects and DC subjects. Through our work, we contribute towards an enhanced understanding of ASD, potentially paving the way for future research and therapeutic interventions.**

***Keywords*—Autism spectrum disorder (ASD); Magnetic Resonance Imaging (MRI); functional Magnetic Resonance Imaging (fMRI); Artificial Neural Network (ANN)**

I. Introduction

The nature of Autism Spectrum Disorder (ASD) is multilayered and intriguing, with its diverse manifestations affecting various aspects of an individual's life[1]. From social communication and behavioral patterns to intellectual abilities, ASD presents an array of symptoms that make it a unique neurodevelopmental disorder. An estimated one in every 54 children is affected by ASD globally, underscoring its significant prevalence [2]. Despite this high occurrence, the causes of ASD remain enigmatic. Multiple genetic and environmental risk factors have been identified, yet they only partially explain the incidence of ASD. Consequently, rigorous research efforts continue to seek a deeper understanding of ASD's intricate etiology and neurobiology.

Advancements in the field of neuroimaging have significantly contributed to our understanding of neurodevelopmental disorders such as ASD. From purely descriptive studies of the brain's anatomy, neuroimaging research has evolved to explore the profound neurodevelopmental alterations that occur in these conditions. Modern imaging techniques such as Structural Magnetic Resonance Imaging (sMRI) and functional Magnetic Resonance Imaging (fMRI), combined with state-of-the-art computational tools and machine learning algorithms, have provided unprecedented insights into the structural and functional anomalies associated with neurodevelopmental disorders. This development has brought about a paradigm shift in our understanding of these conditions, with a newfound focus on identifying potential biomarkers that can serve as quantitative indicators of specific brain abnormalities.

MRI is an indispensable tool in ASD research, enabling non-invasive imaging of brain structure, connectivity, and function. Structural MRI studies have identified various alterations in brain regions involved in social communication, language processing, executive functions, and sensory integration in individuals with ASD. Functional MRI, on the other hand, has been pivotal in uncovering disrupted functional connectivity, particularly in regions responsible for social cognition and emotion processing. MRI's widespread utilization in ASD research has undoubtedly been instrumental in enhancing our understanding of the disorder's neurobiology.

In-depth analysis of specific neuroanatomical regions has revealed that ASD is associated with certain alterations in brain structure, contributing to the varied cognitive and behavioral phenotypes observed in these individuals. Volumetric analysis of specific brain regions has reported differences in brain volumes between individuals with ASD and typically developing individuals. Similarly, cortical thickness analysis has identified disparities in the cerebral cortex's thickness between these two groups. The integration of these structural findings with functional studies has resulted in a holistic

understanding of the neurobiological underpinnings of ASD (Appendix A)

Our research aims to extend these efforts by considering all the neuroanatomical regions implicated in ASD. Utilizing a sophisticated automated processing pipeline, we perform a comprehensive analysis of both 3D volumetric and functional brain regions. This inclusive approach ensures that we capture the full range of structural and functional abnormalities associated with ASD. Our work incorporates texture features derived from global descriptors and local textural features for the structural analysis, combined with statistical and temporal features for the functional analysis. This holistic approach allows us to identify unique volumetric and functional signatures of ASD, with the potential to contribute significantly to early detection, diagnosis, and monitoring of the disorder.

The organization of this paper is as follows: Section II delineates the primary methodology used in our study, encompassing both structural and functional analyses. In Section III, we present the outcomes of our research, along with a thorough discussion on the effectiveness and implications of our proposed approach. The limitations of our study are discussed in Section IV. Finally, we draw conclusions from our findings in Section V.

II. Materials and Methods

This chapter elaborates on the methods utilized in our study to distinguish autism using MRI and fMRI data. Initially, we detail the preprocessing steps for data standardization. Then, we describe how significant features were extracted from the imaging data. Finally, we explain the classification techniques used to differentiate between autistic and neurotypical individuals. This approach allows us to identify potential autism biomarkers and understand the underlying neural mechanisms. You will find the pipeline of our structural method in the Fig. 1.

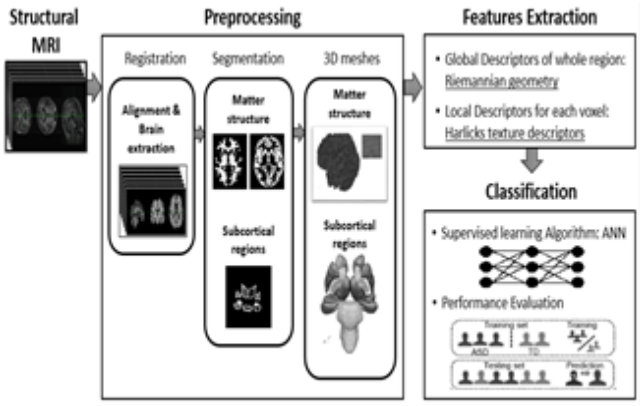

Fig. 1. Pipeline of the structural analysis methods for the characterization of ASD.

A. Structural Analysis

- Preprocessing of sMRI

MRI registration is a key step in neuroimaging studies, aligning multiple MRI images for spatial correspondence. Commonly, the Montreal Neurological Institute space (MNI 152 space) is used as a reference for this alignment. This process involves an initial reorientation of MRI scans, with anatomical labels defined to correct any discrepancies. Then, we perform a skull stripping or brain extraction step to isolate brain tissue from non-brain elements, using methods like the Optimal Surface Thresholding (OST). This step is crucial in reducing potential artifacts in subsequent MRI analyses (Fig. 2).

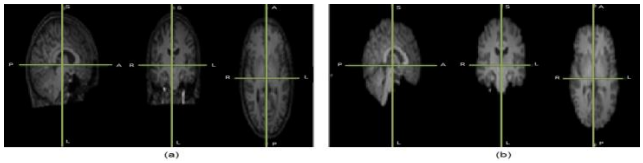

Fig. 2. An example of the brain MRI registration with an original MR image of brain (a) and registered image (b).

- Segmentation of the Regions of Interest

In our research, we apply an automatic method for identifying and segmenting brain regions of interest (Appendix B) relevant to ASD using both probabilistic and anatomical models. A Bayesian probabilistic approach, based on Markov modeling, is used for accurate identification and segmentation of ROIs. This approach incorporates prior knowledge about brain structures, facilitating accurate ROI identification. Markov random fields (MRFs) account for spatial dependencies between neighboring elements in the image, enforcing spatial continuity and reducing the impact of noise[3].

$$P(A|B) = (P(B|A) * P(A))/P(B) \quad (1)$$

Where:

P(A | B) is the posterior probability of event A occurring, given that event B has occurred.

P(B | A) is the likelihood of event B occurring, given that event A has occurred.

P(A) is the prior probability of event A occurring.

P(B) is the marginal probability of event B occurring.

The process involves formulating a model incorporating Bayesian probability theory and Markov models, estimating model parameters using the maximum likelihood estimation (MLE), and iteratively refining the model using the Expectation-Maximization (EM) algorithm[4]. The final step is image classification and segmentation using maximum a posteriori (MAP) estimation, assigning each pixel or voxel to a specific ROI based on the most probable assignment given the observed data and the model parameters.

$$MLE\ (\theta) = argmax(P(X|\theta)) \quad (2)$$

where θ represents the model parameters, X denotes the observed data, and P(X | θ) is the likelihood of the data given the parameters. During this process, we account for the natural variability in the image data and consider the spatial dependencies between neighboring elements[5].

$$MAP(\theta) = argmax\big(P(\theta|X)\big) \quad (3)$$

where θ represents the model parameters, X denotes the observed data, and P(θ | X) is the posterior probability of the parameters given the data (result in Fig. 3).

Fig. 3. Segmentation steps of left hippocampus.

- 3D mesh construction

Medical imaging and computer vision often require the transformation of raw image data into a format more suitable for analysis, and 3D mesh models fill this need. The process begins with image segmentation, followed by surface extraction, and finally, mesh generation. The surface of the target object is extracted using the Marching Cubes algorithm, which divides the 3D volume into a grid of small cubes and forms a polygon configuration within each cube based on whether corners lie above or below a certain threshold. This creates an interconnected surface approximating the boundary of the target structure.

Next, mesh generation connects points on the surface to form polygons in a process known as triangulation, resulting in a 3D mesh composed of numerous triangles. This mesh model, which represents the 3D shape of the target object, provides a detailed and accurate foundation for further analysis, visualization, or computation (result in Fig. 4).

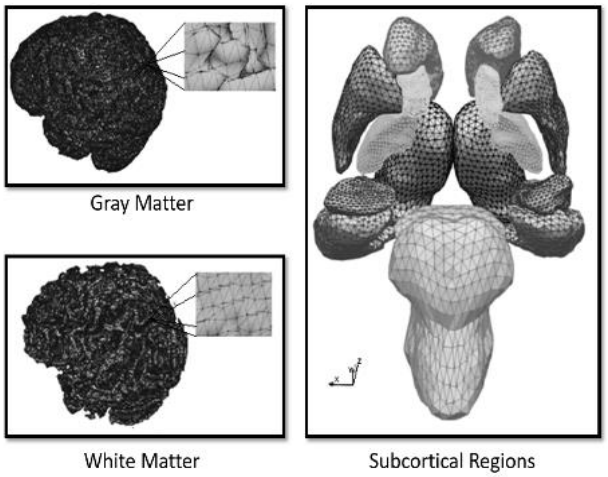

Fig. 4. 3D Meshes structures.

- Feature extraction of sMRI

The analysis of anatomical MRI data involves a pivotal phase known as feature extraction. This step translates complex 3D images into measurable, actionable information by identifying and quantifying various properties of the structures within the images. This process plays an integral role in exploring potential biomarkers for Autism Spectrum Disorder (ASD). Feature extraction focuses on two primary categories: geometric and texture features.

Geometric features provide information about the shape and structure of areas within the brain, helping to understand physical alterations related to ASD. Texture features, on the other hand, capture intensity variations within a region, revealing patterns that might indicate different tissue types or states, and possibly reflecting microstructural properties of the brain regions linked to neurodevelopmental changes in ASD.

In this study, multiple mathematical and statistical methods are applied to calculate these features. Riemannian geometry is used to understand the intrinsic curvature of surfaces and spaces. It allows for the computation of the area, volume, isoperimetric ratio, convexity ratio of the surface and volume, and Gaussian and Mean curvatures.

Haralick texture features, or Gray Level Co-occurrence Matrix (GLCM) features, provide a statistical snapshot of the texture. Several statistical measures are derived from the GLCM, including the Angular Second Moment (or Energy), Contrast, Correlation, Variance, Inverse Difference Moment (or Homogeneity), Entropy, Sum Average, Sum Variance, Sum Entropy, Difference Variance, and Difference Entropy (Annex B).

By combining geometric and texture feature extraction, a comprehensive picture of the structural changes associated with ASD is captured. This approach goes beyond traditional measures and explores a broader spectrum of potential biomarkers. Through statistical analysis of these features, patterns can be identified that could serve as reliable biomarkers for ASD, enhancing our understanding of this complex condition and potentially informing future diagnostic and therapeutic strategies.

B. Functional Analysis

- Preprocessing of fMRI

The preprocessing of fMRI data begins with obtaining raw scan data. This data then undergoes several steps to enhance its quality and reliability (Fig. 5). These steps include:

Motion Correction: This process is used to minimize the effects of head movement during the scan. The process involves realigning all volumes acquired during an fMRI scan to a reference volume to eliminate motion-related artifacts.

Slice Timing Correction: This step compensates for the time difference between the acquisitions of different slices in each volume. The correction aims to align the signal from all slices as if they were acquired at the same time, improving the accuracy of the data.

Registration: This process aligns different sets of data into one common space. It involves within-subject registration (aligning images from the same individual) and between-subject registration (aligning images from different individuals to a standard template).

Spatial Normalization: This involves transforming individual brain images to fit into a standard template, enabling group analyses and inter-subject comparisons.

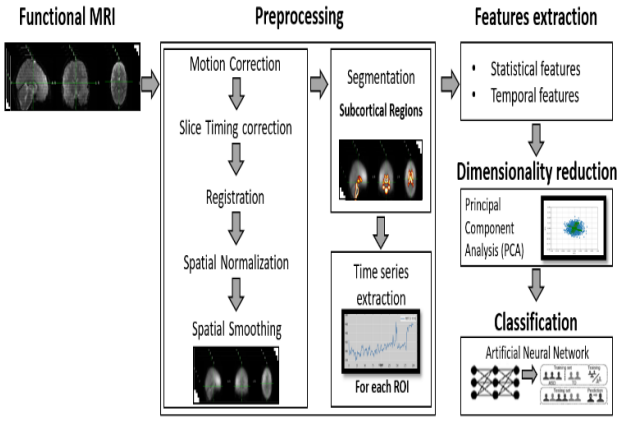

Fig. 5. Pipeline of the functional analysis methods for the characterization of ASD.

Spatial Smoothing: This process improves the signal-to-noise ratio by averaging a voxel's signal with the signal of surrounding voxels. It also helps mitigate differences in functional neuroanatomy across participants and satisfies certain statistical assumptions (result in Fig. 6).

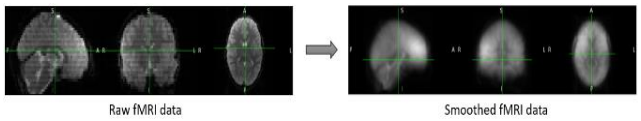

Fig. 6. Example of preprocessing data.

- Segmentation of the Regions of Interest

In our autism study, we furthered our fMRI data analysis by segmenting regions of interest (ROIs), focusing specifically on brain regions previously implicated in autism spectrum disorder (ASD). This approach allowed us to investigate how structural abnormalities in these regions may influence functional connectivity patterns and contribute to ASD's characteristic features (Fig. 7).

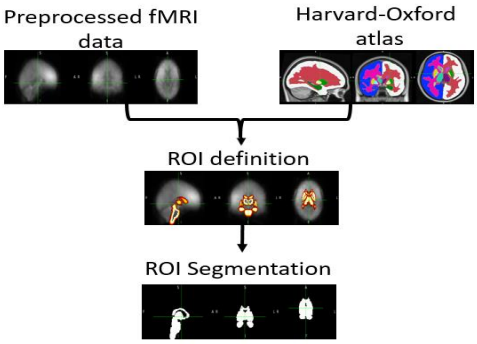

Fig. 7. ROI segmentation.

To achieve this, we utilized Atlas-based segmentation, employing the Harvard-Oxford atlas for its detailed labeling of cortical and subcortical brain structures. After selecting our ROIs from this atlas, we applied the labels to our fMRI data through a process known as label propagation. The segmentation information from multiple atlas images, when used, was fused to create the final segmentation result. This thorough process ensured accurate segmentation and paved the way for our subsequent ASD analysis and classification.

- Time Series Extraction

After defining the regions of interest (ROIs) in our fMRI data, we conducted time-series extraction, a fundamental step in functional connectivity analysis. This process involves gathering the intensity values for each voxel within the ROI across each time point in the fMRI series. By averaging the signal change over time across all voxels within each ROI, we generated a single time-series for each region, enabling us to investigate various patterns of brain activity over time (Fig. 8).

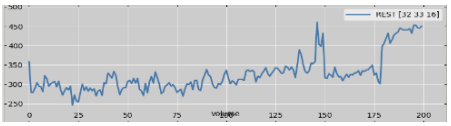

Fig. 8. Example of time series for one voxel.

- Feature extraction of fMRI

In our analysis of fMRI data, we performed feature extraction, a process to convert raw, high-dimensional time series data into a simpler, lower-dimensional format. We used the Python library tsfresh to extract 150 statistical and temporal features from the time series data.

Statistical features provided a summarized description of the variation in signal intensity over time. They included measures like mean, median, variance, standard deviation, and others, helping to quantify the properties of the signal.

Temporal features captured how brain responses changed over the course of the experiment. They included Autoregression coefficients, trend features, and Fourier coefficients among others, allowing us to uncover patterns in brain activity and comprehend the interactions between different brain regions.

Through feature extraction, we transformed complex fMRI data into a more manageable format without losing vital information, preparing it for processing by machine learning models.

C. Multi-Modal Imaging Fusion

In this section of our research, we'll take the critical step of fusing the feature sets derived from both structural and functional imaging data. This combined feature set will be utilized to provide a comprehensive perspective on the neuroanatomy and functionality of the key brain regions implicated in Autism Spectrum Disorder (ASD). This integrated analysis could provide more robust and meaningful insights into the neurobiological underpinnings of ASD.

- Dimensionality reduction

Upon combining the features extracted from both the structural and functional data, we find ourselves dealing with an extremely high-dimensional feature set. This poses a significant challenge in the context of machine learning, potentially leading to overfitting, difficulty in interpretation, and a spike in computational demands. This is where feature selection comes into play.

Feature selection allows us to filter out less informative features and focus on those that contribute the most to our model's predictive power. We utilized Principal Component Analysis (PCA) as a strategic choice for our feature selection process. PCA is particularly advantageous for our high-dimensional data as it allows us to reduce the dimensionality while retaining as much information as possible. PCA identifies the directions (principal components) in which the data varies the most and transforms the original, high-dimensional data into a lower-dimensional set of new features, Fig. 9. These features are linear combinations of the original ones, selected in such a way that they are uncorrelated and retain the maximum amount of variance from the original data.

In our study, we set the PCA to retain 95% of the variance. This criterion led to the selection of 30 principal components which are sufficient to retain 95% of the information from the original features. The resulting dataset, composed of 30 uncorrelated principal components, still captures the major patterns and structures in our original high-dimensional data, making it a more manageable and effective input for our subsequent machine learning model. Thus, the application of PCA serves as a powerful step in preparing our feature set for the final stages of ASD diagnosis.

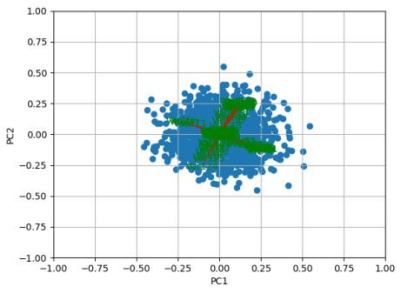

Fig. 9. Feature contributions to the first two principal components.

- Classification

Classification is essential in diagnosing ASD using machine learning. We've chosen to employ an Artificial Neural Network (ANN), a model that imitates the human brain's structure and function, for this task. ANNs consist of interconnected neurons in layers: an input layer for receiving data, hidden layers for data processing, and an output layer for final results. ANNs 'learn' by adjusting inter-neuron connections through backpropagation, thereby minimizing the difference between predicted and actual outputs. Their ability to model complex, non-linear relationships and learn intricate patterns make ANNs an effective tool for accurate ASD classification, given enough data and training time.

In our study, we applied an ANN for ASD classification, guided by an intricate process. Firstly, we initiate feedforward computation, where the input is sequentially processed through each layer of the network using a sigmoid activation function. The final prediction is made at the output layer. We then employ a loss function, specifically Mean Squared Error (MSE), to quantify the discrepancy between the network's prediction and the actual value[6].

$$MSE = \frac{1}{N}\sum_{i=1}^{N}(y_i - \hat{y}_i)^2 \quad (4)$$

Where:

N is the number of samples

y_i is the actual value

$\hat{y}_i$ is the predicted value

The loss function thereby indicates the error of the network. Backpropagation, a method of calculating the loss function's gradient with respect to the network's weights and biases, follows. It commences from the output layer, moving backward through the hidden layers. The network's weights and biases are then updated by subtracting a fraction of the gradient, dictated by the learning rate, a key hyperparameters. This whole process is repeated for each batch of data in the training dataset for a set number of epochs, gradually adjusting the network's weights and biases to minimize the loss function, and improving prediction accuracy. We customized certain hyperparameters (Appendix C, Table VII), like the learning rate and the structure of hidden layers, for our specific application to ensure optimal performance. By fine-tuning these hyperparameters, we could better capture complex patterns in ASD data, thereby increasing the accuracy of our ASD characterization (Fig. 10).

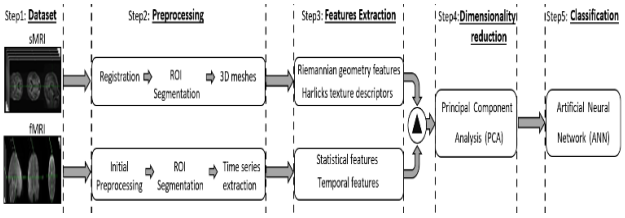

Fig. 10. Pipeline of diffusion method.

III. Results and Discussion

In this section, we initially outline the database utilized for our investigation in the first part. This is followed by a description of the tuning process for the ANN in Section B. Subsequently, we delve into an evaluation of the proposed method's performance. Lastly, we provide a comparative analysis with a few prevalent techniques from the established standards.

A. Database Description

The non-invasive imaging technique, MRI is pivotal to our study for its ability to generate detailed, high-resolution images of the brain. Our investigation uses data from the Autism Brain Imaging Data Exchange (ABIDE), a collaborative initiative that curates diverse MRI datasets globally for autism research. This collaboration ensures a robust dataset that offers comprehensive insight into autism's structural patterns.

ABIDE provides a large-scale collection of both structural and functional MRI datasets, improving our understanding of the neural mechanisms underlying ASD. With over 1200 datasets from more than 24 international brain imaging laboratories, these collections afford a rich assortment of data for our analyses.

In our work, the ABIDE data is categorized into three distinct age groups - early childhood (1-9 years), late childhood and adolescence (10-25 years), and adulthood (above 25

years), each reflecting a different stage of brain development, Table I. This classification allows us to examine autism's manifestation and evolution throughout life stages, offering a nuanced understanding of ASD's progression and neurological implications.

TABLE I. THE DEMOGRAPHIC INFORMATION OF THE DATABASE ABIDE

1st range		2nd range		3rd range	
The postnatal development of the human brain.		***The brain reaches its adult size.***		***The brain reaches its full size.***	
5-9 years old		10-25 years old		+25 years old	
646 patients		218 patients		148 patient	
315 ASD	331 NC	154 ASD	164 NC	70 ASD	78 NC

B. Machine Learning Evaluation

- k-fold cross-validation

Our study applies probabilistic learning methods to optimize neural networks, dividing our data into training and testing sets for reliable model training and validation. The training set is used to teach the model to recognize data patterns, while the unseen testing set assesses how well it generalizes these patterns. We employ k-fold cross-validation to bolster the reliability of our results and avoid overfitting. This involves splitting the training data into 'k' subsets and training the model 'k' times, each time using a different subset for validation (Fig. 11).

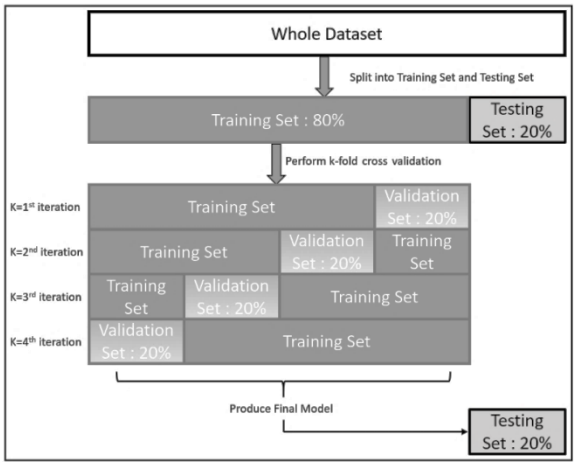

Fig. 11. How the dataset was split.

This provides 'k' models and performance estimates which can be averaged to offer a more reliable measure of performance. Specifically, we use 4-fold cross-validation, partitioning our data into four subsets. For each training cycle, 80% of the data trains the model, while the remaining 20% validates it. The model's performance is then assessed using the validation set, and quantified using metrics such as accuracy, precision, and recall. By averaging performance across four iterations, we gain a robust measure of the model's predictive capabilities, mitigating the risk of overfitting and providing a realistic evaluation of the model's potential real-world performance. This approach ensures the robustness, reliability, and applicability of our model in studying autism spectrum disorders.

- Performance evaluation

In our study, we use an ANN classifier to analyze features derived from structural and functional MRI data. The analysis reveals differences in specific brain regions when compared to a control group[7]. The model's performance, evaluated using the identified feature sets, is detailed in Table II, which demonstrate metrics like accuracy, sensitivity, and specificity.

Accuracy is a simple performance metric, calculated as the ratio of correct model predictions to total predictions. Ranging between 0 and 1, a score of 1 denotes a perfect model. We use the equation:

$$Accuracy = (TP + TN)/(TP + FP + FN + TN) \quad (5)$$

where TP, TN, FP, and FN represent true positives, true negatives, false positives, and false negatives, respectively.

Sensitivity, or recall, measures the proportion of actual positive cases correctly identified by the model. Calculated as:

$$Sensitivity = TP/(TP + FN) \quad (6)$$

It quantifies the model's ability to detect all relevant instances.

Specificity evaluates the model's performance regarding negative cases. It represents the proportion of true negative cases correctly identified by the model, computed as:

$$Specificity = TN/(TN + FP) \quad (7)$$

By using these three metrics to evaluate our model, we ensure that it is well-rounded, accurately predicting both positive and negative cases. This makes it a potentially valuable tool in characterizing autism.

- Results

In our study, we evaluate the effectiveness of an ANN in differentiating between individuals diagnosed with ASD and control subjects across various age groups. This evaluation employs a fusion of structural and functional analyses, a crucial approach for comprehensively understanding the relationships within the brain's structure-function framework. We base this assessment on a combination of geometric, volumetric, temporal, and statistical features, the outcomes of which are represented in Tables II, III, and IV.

- Discussion

In this research, we utilize an ANN to differentiate individuals diagnosed with ASD from control subjects across various stages of life: early childhood, late childhood and adolescence, and adulthood. Both structural and functional characteristics of the brain are examined to provide a comprehensive view of how our model performs. By integrating both structural and functional neural features, our classifier demonstrated robust performance across all developmental stages. Despite a decline in accuracy with increasing age, the integrated approach provided valuable insights, highlighting the relevance of a comprehensive brain analysis in diagnosing ASD.

TABLE II. EVALUATION RESULTS OF THE FIRST RANGE AGED FROM 5 YEARS TO 9 YEARS

Region	WB	GM	Left Pa	Left NA	Left Thala	Left Amy	Left Pu	Left Hipp	Left CN	Left CC
Accuracy	81.2	79.7	70.9	77.5	80.9	89.2	79.2	88.5	72.5	88.3
Sensitivity	0.86	0.72	0.88	0.70	0.82	0.90	0.82	0.92	0.95	0.89
Specificity	0.59	0.66	0.57	0.61	0.66	0.70	0.60	0.69	0.75	0.74
Region	**B.Stem**	**WM**	**Right Pa**	**Right NA**	**Right Thala**	**Right Amy**	**Right Pu**	**Right Hipp**	**Right CN**	**Right CC**
Accuracy	87.0	77.9	78.6	77.5	77.6	90.5	79.9	89.4	75.9	88.6
Sensitivity	0.85	0.88	0.72	0.90	0.89	0.83	0.77	0.80	0.75	0.80
Specificity	0.70	0.58	0.62	0.77	0.65	0.76	0.85	0.79	0.60	0.66
Fusing all ROI: accuracy =90.1%										

TABLE III. EVALUATION RESULTS OF THE FIRST RANGE AGED FROM 10 YEARS TO 25 YEARS

Region	WB	GM	Left Pa	Left NA	Left Thala	Left Amy	Left Pu	Left Hipp	Left CN	Left CC
Accuracy	73.0	72.7	63.0	71.9	73.2	81.2	78.6	85.2	83.0	79.6
Sensitivity	0.80	0.70	0.73	0.81	0.69	0.74	0.58	0.84	0.77	0.88
Specificity	0.63	0.56	0.59	0.44	0.55	0.63	0.47	0.65	0.45	0.79
Region	**B.Stem**	**WM**	**Right Pa**	**Right NA**	**Right Thala**	**Right Amy**	**Right Pu**	**Right Hipp**	**Right CN**	**Right CC**
Accuracy	69.7	78.3	70.0	68.4	69.0	85.1	70.4	84.2	69.9	77.9
Sensitivity	0.69	0.72	0.72	0.90	0.82	0.88	0.83	0.76	0.65	0.58
Specificity	0.70	0.60	0.64	0.47	0.60	0.53	0.52	0.63	0.74	0.47
Fusing all ROI: accuracy =86.2%										

TABLE IV. EVALUATION RESULTS OF THE FIRST RANGE AGED FROM 26 YEARS TO 64 YEARS

Region	WB	GM	Left Pa	Left NA	Left Thala	Left Amy	Left Pu	Left Hipp	Left CN	Left CC
Accuracy	56.2	46.8	59.1	61.5	57.2	57.8	65.4	59.2	59.0	62.1
Sensitivity	0.61	0.71	0.54	0.75	0.63	0.78	0.59	0.79	0.70	0.79
Specificity	0.47	0.35	0.69	0.59	0.54	0.65	0.72	0.51	0.54	0.58
Region	**B.Stem**	**WM**	**Right Pa**	**Right NA**	**Right Thala**	**Right Amy**	**Right Pu**	**Right Hipp**	**Right CN**	**Right CC**
Accuracy	50.9	50.1	55.4	50.8	62.1	56.5	54.5	62.0	53.1	59.9
Sensitivity	0.83	0.72	0.62	0.75	0.59	0.63	0.70	0.92	0.55	0.88
Specificity	0.59	0.51	0.64	0.60	0.71	0.74	0.56	0.66	0.75	0.68
Fusing all ROI: accuracy =67.9%										

The combined analysis in the late childhood and adolescence stage maintains high accuracy levels, with the right amygdala again leading with an accuracy of 85.1%. The accuracy levels of WB and GM are 73.0% and 72.7%, respectively. While the accuracy rates have declined slightly from the early childhood stage, the fused ROI result still maintains a solid accuracy of 86.2%.

The final findings underscore the complexity of ASD and the importance of a multifaceted approach to brain data analysis for accurate ASD identification. The research provides a promising pathway for the future of ASD detection and diagnosis, and potentially for other neurodevelopmental and neurodegenerative disorders, through the use of ANN classifiers. Our methodology, which combines structural and functional brain properties, could serve as a valuable tool in the development of Computer-Aided Diagnosis systems, particularly for neurodegenerative diseases like Alzheimer's and Parkinson's, which also involve significant changes in the brain.

- Comparison analysis

In the table below, we present a comparison of various prior studies that have focused on the characterization of ASD by employing both structural and functional MRI. This comparative analysis aims to provide a broader perspective on how our approach to ASD classification using an ANN stands in relation to previous research efforts.

Each study listed in the table has contributed significantly to our current understanding of ASD's neurological underpinnings. However, the methodologies employed, the specific features extracted, and the performance metrics achieved vary from one study to another. Some researchers have concentrated more on the structural aspects of the brain (Table V), while others have leaned towards functional analysis (Table VI).

TABLE V. ASD CLASSIFICATION STUDIES BASED ON SMRI DATA

Study	Participants	Data	Features	Machine learning method	Accuracy
Seyedmehdi Payabvash, et al.[8]	14 with ASD 33 typically developing children	The UCSF Sensory Neurodevelopment and Autism Program clinical sites and research database	Tract-based average TI/connectome metrics	Support vector machines	75.3%
Almeida, J.,et al.[9]	403 ASD 468 TC	The open database Autism Brain Imaging Data Exchange (ABIDE).	The volume of the cerebral cortex	Support vector machines	76%
Ahmad Chaddad,et al.[10]	34 ASD 30 DC	The open database Autism Brain Imaging Data Exchange (ABIDE).	11 features derived from Hippocampus Amygdala	Support vector machines	67.85%
Ayşe Demirhan et al.[11]	1390 subjects	Five different datasets : OASIS, ABIDE, COBRE, ADHD and MCIC	Volumes and thickness of anatomical structures	Support vector machines	83%
Pinaya et al.[12]	HC=105 ASD=83	Autism Brain Imaging Data Exchange (ABIDE) data set	ROI based volumetric measurements	Deep autoencoder	63.9%
Ferrari et al.[13]	HC=1166 ASD=1060	T1w from ABIDE I and ABIDE II	Brain morphometric features	Deep autoencoder	79%
Qureshi, M.N.I.et al[14]	1000 subjects	Attention deficit hyperactivity disorder ADHD-200 dataset of patients and healthy children.	the cortical thickness measures	Support vector machines	76.19%
Xiao, X.et al[15]	46 ASD 39 DC	Child Mental Health Research Center of Nanjing Brain Hospital	cortical-thickness measurement surface-based morphometry	RF NB SVM	75.6% 80.9% 80%
Sina Ghiassian.et al[16]	490 HC 279 ASD	Attention deficit hyperactivity disorder ADHD-200 dataset of patients and healthy children.	HOG feature extraction	Support vector machines	69.6%
Dennis Dimond et al.[17]	27 ASD 31 TD	Participant databases at the Alberta Children's Hospital	intra-cranial volume	Artificial Neural Network	77%
Bhashkar Sen, et al[18]	ADHD: 491 HC et 279 ASD ABIDE: 573 HC et 538 ASD	ADHD-200 (including 8 sites) ABIDE (including 17 sites)	3-D texture based and independent component analysis	Linear support vector machine classifier	ADHD 0.64% ABIDE 0.62%
Calderoni et al[19]	HC=19 ASD=38	T1w	voxel-based morphometry (VBM)	Support vector machines	80%
Gori et al[20]	HC=20 ASD=21	T1w	Regional morphological features	Support vector machines	74%
Hossein Shahamat et al[21]	403 ASD 468 TC	Autism Brain Imaging Data Exchange (ABIDE) data set: 1112 datasets		Convolutional neural network (CNN) models	70%
Guannan LI et al.[22]	170 TC 106 ASD	276 subjects from National Database for Autism Research (NDAR)		3D Convolutional neural network (CNN) models	0.7624
Fengkai Ke et al[23]	ADHD: 40 HC 33 ASD ABIDE: 573 HC 538 ASD	The first dataset was collected by the Yonsei University College of Medicine (YUM) + the second was ABIDE dataset		3D CNN	0.64

TABLE VI. ASD CLASSIFICATION STUDIES BASED ON RS-FMRI DATA

Study	Participants	Data	Features	Feature selection	Machine learning method	Accuracy
Reiter et al. (2021) [24]	306 ASD 350 TC	rs-fMRI data(the ABIDE dataset and data sample from SDSU)	FC between 237 ROIs (the Gordon atlas the HO atlas)	Conditional random forest	Random Forest	62.5% 65% 70% 73.75%
Yang et al. (2021) [25]	79 ASD 105 TC	rs-fMRI data (the ABIDE dataset)	8 brain functional networks from group-ICA	Dual regression	3D CNN classifier	77.74%
Kazeminejad and Sotero (2020) [26]	493 ASD 530 TC	rs-fMRI data (the ABIDE dataset)	FCs between 200 ROIs (the CC200 atlas)	PCA	A multilayer perceptron	64.4%
Liu Y. et al. (2020) [27]	403 ASD 468 TC	rs-fMRI data (the ABIDE dataset)	D- FCs between ROIs (the AAL atlas)	MTFS-EM	Multi-kernel SVM	76.8%
Huang et al. (2020) [28]	505 ASD 530 TC	rs-fMRI data (the ABIDE dataset)	FCs between 200 ROIs (the CC200 atlas)	Graph-based feature-selection method	DBN classifier	76.4%
Thomas et al. (2020) [29]	620 ASD 542 TC	rs-fMRI data (the ABIDE dataset)	Nine summary measures	None	3D CNN classifier	64%
Sherkatghanad et al. (2020) [30]	505 ASD 530 TC	rs-fMRI data (the ABIDE dataset)	FCs between 392 ROIs (the CC400 atlas)	None	CNN classifier	70.22%
Liu Y. et al. (2020)[31]	506 ASD 548 TC	rs-fMRI data (the ABIDE dataset)	FCs between 200 ROIs (the CC200 atlas)	Extra-tree	Linear-SVM	72.2%
Tang et al. (2020) [32]	505 ASD 530 TC	rs-fMRI data (the ABIDE dataset)	FCs between 116 ROIs fMRI × ROI connectivity (the AAL atlas)	None	DNN classifier	74%
Fredo et al. (2019) [33]	306 ASD 350 TC (400 participants for each sample)	rs-fMRI (the ABIDE dataset)	FCs between 237 ROIs (the Gordon's cortical atlas the HO atlas)	Conditional random forest	Random forest	62.5% 65% 70% 73.75%
Eslami et al. (2019) [34]	505 ASD 530 TC	rs-fMRI data (the ABIDE dataset)	FCs between 200 ROIs (the CC200 atlas)	AE	A single layer perceptron	80%
Kazeminejad and Sotero (2019) [35]	109 participants 342 participants 190 participants 137 participants 51 participants	rs-fMRI data (the ABIDE dataset)	FCs between 116 ROIs (the AAL atlas)	A sequential forward floating algorithm	Gaussian SVM	86% 69% 78% 80%
Li et al. (2018) [36]	38 ASD 23 TC	rs-fMRI data (the ABIDE dataset)	FCs between 90 ROIs (the AAL atlas)	SSAE	DTL-NN classifier	70.4%

This comparison underscores the diverse approaches researchers have taken to tackle ASD classification using MRI data. Our research's contribution lies in its unique fusion of both structural and functional analyses across different age groups, which provides a more holistic understanding of ASD's neurological characteristics. The table below offers a succinct summary of these various studies, illuminating the varying methodologies and results that have been achieved in the past.

IV. STUDY LIMITATIONS

Despite the promising findings, the current study is not without its limitations. Primarily, our work relies on the Autism Brain Imaging Data Exchange (ABIDE) which, while being a rich public dataset, has its limitations. The datasets are collected from 521 individuals with ASD and 593 controls with ages ranging from five to 64 years. However, this is a comparatively small dataset for making definitive classifications. To expand upon the insights provided by this study, future research should aim to collect data from a larger group of preschoolers with ASD to further explore brain development during early childhood.

Secondly, while we acknowledge the gender disparity in ASD diagnoses, with males being more frequently diagnosed than females, this issue has been generally overlooked in ASD imaging literature due to the significantly higher prevalence of ASD in males. In the ABIDE dataset, the number of datasets from females is limited (65 datasets, encompassing both ASD and control subjects), making a thorough analysis of gender influences challenging. Despite the potential of Artificial Neural Networks (ANNs), they have inherent limitations. Their 'black-box' nature makes it hard to understand how they arrive at specific predictions, leading to challenges in interpretability. Furthermore, ANNs can sometimes overfit high-dimensional data, especially with limited samples, leading to poor performance on unseen data. To address these issues, future work could explore methods for enhancing interpretability and preventing overfitting.

While these limitations pose challenges, they also highlight potential directions for future research. We need larger, more

diverse samples and more robust methods to handle high-dimensional data for more accurate and generalizable results. In addition, research efforts should not neglect gender disparities in ASD and strive for greater representation in imaging studies. By addressing these issues, we can further refine our understanding of ASD's neurobiological underpinnings and improve diagnostic strategies.

V. CONCLUSION

In conclusion, our study has successfully highlighted the significance and value of employing an integrated, multimodal approach in characterizing and diagnosing ASD across various developmental stages. The results have underscored the vital role played by specific brain regions such as the Right Amygdala, Left Amygdala, Right Corpus Callosum, Left Putamen, and Right Hippocampus in ASD classification. Furthermore, the distinctive combination of both structural and functional neural features in our ANN classifier has proven to be a powerful tool in capturing the complex neurobiological nuances of ASD.

While the classifier demonstrated robust performance across all developmental stages, particularly in early childhood, it also unveiled the increasing complexity of ASD diagnosis in later life stages. This highlights the intricate interplay between ASD symptomatology, brain development, and aging. However, even amidst these challenges, the classifier continued to provide valuable insights and significant accuracy scores, asserting the value of a comprehensive brain analysis approach for ASD diagnosis.

The fusion of results from structural and functional analyses created a more comprehensive model for ASD classification, resulting in a more robust and accurate representation of the disorder. This integrated approach produced promising results, especially in the domain of early ASD diagnosis. The highest diagnostic accuracy achieved in our study reached 90.1%, signifying the potential of a multimodal approach that captures a more complete picture of ASD's neurobiological underpinnings.

Our study contributes significantly to the field by providing a broader understanding of ASD. By integrating structural and functional aspects of brain imaging data, we enhance our ability to identify and diagnose the disorder accurately. Our research not only paves the way for further advancements in early detection and personalized treatment strategies for individuals with ASD but also sets the stage for this methodology to serve as a Computer-Aided Diagnosis tool for the detection of other neurodegenerative diseases such as Alzheimer's and Parkinson's.

Despite some limitations, particularly regarding the decline in accuracy with increasing age, our study reaffirms the need for a comprehensive, multidimensional analysis of brain data for accurate ASD identification. It also suggests areas for future research to enhance the understanding and diagnosis of ASD, potentially through the development of more sophisticated feature extraction or classification methods.

In essence, this research demonstrates the potential of a comprehensive, multimodal neuroimaging approach, combined with advanced machine learning techniques, to improve early detection and understanding of ASD, thereby paving the way for more effective intervention strategies. It lays a solid foundation for similar techniques to be used for other neurodevelopmental and neurodegenerative diseases, offering a significant tool for future diagnostic strategies.

REFERENCES

[1] C. Lord, M. Elsabbagh, G. Baird, et J. Veenstra-Vanderweele, “Autism spectrum disorder ”, The Lancet, vol. 392, no 10146, p. 508-520, août 2018.

[2] Mandy K. Cohen, MD, MPH “ Data and Statistics on Autism Spectrum Disorder | CDC ”, Centers for Disease Control and Prevention, 12 mai 2023.

[3] A. G. Rubin John B. Carlin, Hal S. Stern, David B. Dunson, Aki Vehtari, Donald B., “Bayesian Data Analysis ”, 3e éd. New York: Chapman and Hall/CRC, 2015.

[4] C. M. Bishop, “Pattern recognition and machine learning. in Information science and statistics ”. New York: Springer, 2006.

[5] K. P. Murphy, “Machine learning: a probabilistic perspective. in Adaptive computation and machine learning series.” Cambridge, MA: MIT Press, 2012.

[6] T. Hastie, R. Tibshirani, et J. Friedman, “The Elements of Statistical Learning. in Springer Series in Statistics. New York, NY: Springer, 2009.

[7] T. Fawcett “An introduction to ROC analysis - ScienceDirect ”. vol.27, no 8, p. 861-874, June 2006.

[8] S. Payabvash et al., “White Matter Connectome Edge Density in Children with Autism Spectrum Disorders: Potential Imaging Biomarkers Using Machine-Learning Models ”, Brain Connect, vol. 9, no 2, p. 209-220, mars 2019.

[9] J. Almeida, N. Velasco, et E. Romero, “A multidimensional feature space for automatic classification of autism spectrum disorders (ASD) ”, vol. 0160, p. 101600X, janv. 2017.

[10] A. Chaddad, C. Desrosiers, L. Hassan, et C. Tanougast, “ Hippocampus and amygdala radiomic biomarkers for the study of autism spectrum disorder ”, BMC Neuroscience, vol. 18, no 1, p. 52, juill. 2017.

[11] A. Demirhan, “The effect of feature selection on multivariate pattern analysis of structural brain MR images ”, Physica Medica, vol. 47, p. 103-111, mars 2018.

[12] W. H. L. Pinaya, A. Mechelli, et J. R. Sato, “Using deep autoencoders to identify abnormal brain structural patterns in neuropsychiatric disorders: A large-scale multi-sample study ”, Hum Brain Mapp, vol. 40, no 3, p. 944-954, oct. 2018.

[13] E. Ferrari et al., “Dealing with confounders and outliers in classification medical studies: The Autism Spectrum Disorders case study ”, Artificial Intelligence in Medicine, vol. 108, p. 101926, août 2020.

[14] M. N. I. Qureshi, J. Oh, B. Min, H. J. Jo, et B. Lee, “Multi-modal, Multi-measure, and Multi-class Discrimination of ADHD with Hierarchical Feature Extraction and Extreme Learning Machine Using Structural and Functional Brain MRI ”, Front Hum Neurosci, vol. 11, p. 157, 2017.

[15] X. Xiao, H.Fang, J. Wu, C. Xiao, T.Xiao, “ Diagnostic model generated by MRI-derived brain features in toddlers with autism spectrum disorder. - Abstract - Europe PMC ”, vol. 15, 30 avril 2021.

[16] M. Liu, B. Li, D.Hu ,“ Using Functional or Structural Magnetic Resonance Images and Personal Characteristic Data to Identify ADHD and Autism ”, 30 avril 2021.

[17] D. Dimond et al., “ Reduced White Matter Fiber Density in Autism Spectrum Disorder ”, Cerebral Cortex, vol. 29, no 4, p. 1778-1788, avr. 2019.

[18] B. Sen, N. C. Borle, R. Greiner, et M. R. G. Brown, “A general prediction model for the detection of ADHD and Autism using structural and functional MRI ”, PLOS ONE, vol. 13, no 4, p. e0194856, avr. 2018.

[19] S. Calderoni, A. Retico, L. Biagi, R. Tancredi, F. Muratori, et M. Tosetti, “ Female children with autism spectrum disorder: An insight from mass-univariate and pattern classification analyses ”, NeuroImage, vol. 59, no 2, p. 1013-1022, janv. 2012.

[20] I. Gori et al., " Gray Matter Alterations in Young Children with Autism Spectrum Disorders: Comparing Morphometry at the Voxel and Regional Level ", Journal of Neuroimaging, vol. 25, no 6, p. 866-874, 2015.

[21] H. Shahamat et M. Saniee Abadeh, "Brain MRI analysis using a deep learning based evolutionary approach ", Neural Networks, vol. 126, p. 218-234, juin 2020.

[22] G. Li, M. Liu, Q. Sun, D. Shen, et L. Wang, "Early Diagnosis of Autism Disease by Multi-channel CNNs ", in Machine Learning in Medical Imaging, Y. Shi, H.-I. Suk, et M. Liu, Éd., in Lecture Notes in Computer Science. Cham: Springer International Publishing, 2018, p. 303-309.

[23] F. Ke, S. Choi, Y. H. Kang, K.-A. Cheon, et S. W. Lee, "Exploring the Structural and Strategic Bases of Autism Spectrum Disorders With Deep Learning ", IEEE Access, vol. 8, p. 153341-153352, 2020.

[24] M. A. Reiter, A. Jahedi, A. R. J. Fredo, I. Fishman, B. Bailey, et R.-A. Müller, " Performance of machine learning classification models of autism using resting-state fMRI is contingent on sample heterogeneity ", Neural Comput & Applic, vol. 33, no 8, p. 3299-3310, avr. 2021.

[25] M. Yang et al., "Large-Scale Brain Functional Network Integration for Discrimination of Autism Using a 3-D Deep Learning Model ", Frontiers in Human Neuroscience, vol. 15, 2021.

[26] A. Kazeminejad et R. C. Sotero, "The Importance of Anti-correlations in Graph Theory Based Classification of Autism Spectrum Disorder ", Frontiers in Neuroscience, vol. 14, 2020.

[27] J. Liu, Y. Sheng, W. Lan, R. Guo, Y. Wang, et J. Wang, " Improved ASD classification using dynamic functional connectivity and multi-task feature selection ", Pattern Recognition Letters, vol. 138, p. 82-87, oct. 2020.

[28] Z. Huang, Z. Zhu, C. Heung Yau, K. Chen Tan, " Identifying Autism Spectrum Disorder From Resting-State fMRI Using Deep Belief Network | IEEE Journals & Magazine | IEEE Xplore ", Jul. 2021.

[29] R. M. Thomas, S. Gallo, L. Cerliani, P. Zhutovsky, A. El-Gazzar, et G. van Wingen, "Classifying Autism Spectrum Disorder Using the Temporal Statistics of Resting-State Functional MRI Data With 3D Convolutional Neural Networks ", Frontiers in Psychiatry, vol. 11, 2020.

[30] Z. Sherkatghanad et al., "Automated Detection of Autism Spectrum Disorder Using a Convolutional Neural Network ", Frontiers in Neuroscience, vol. 13, 2020.

[31] Y. Liu, L. Xu, J. Li, J. Yu, et X. Yu, "Attentional Connectivity-based Prediction of Autism Using Heterogeneous rs-fMRI Data from CC200 Atlas ", Experimental Neurobiology, vol. 29, no 1, p. 27-37, févr. 2020.

[32] M. Tang, P. Kumar, H. Chen, et A. Shrivastava, "Deep Multimodal Learning for the Diagnosis of Autism Spectrum Disorder ", Journal of Imaging, vol. 6, no 6, Art. no 6, juin 2020.

[33] A. R. Jac Fredo, A. Jahedi, M. A. Reiter, et R.-A. Müller, " RETRACTED ARTICLE: Classification of severe autism in fMRI using functional connectivity and conditional random forests ", Neural Comput & Applic, vol. 32, no 12, p. 8415-8415, juin 2020.

[34] Mirjalili, A. Fong, A. R. Laird, et F. Saeed, " ASD-DiagNet: A Hybrid Learning Approach for Detection of Autism Spectrum Disorder Using fMRI Data ", Frontiers in Neuroinformatics, vol. 13, 2019.

[35] A. Kazeminejad et R. C. Sotero, " Topological Properties of Resting-State fMRI Functional Networks Improve Machine Learning-Based Autism Classification ", Frontiers in Neuroscience, vol. 12, 2019.

[36] H. Li, N. A. Parikh, et L. He, " A Novel Transfer Learning Approach to Enhance Deep Neural Network Classification of Brain Functional Connectomes ", Frontiers in Neuroscience, vol. 12, 2018.

[37] H. Ohta et al., "White matter alterations in autism spectrum disorder and attention-deficit/hyperactivity disorder in relation to sensory profile ", Molecular Autism, vol. 11, no 1, p. 77, oct. 2020.

[38] T. P. DeRamus et R. K. Kana, "Anatomical likelihood estimation meta-analysis of grey and white matter anomalies in autism spectrum disorders ", Neuroimage Clin, vol. 7, p. 525-536, nov. 2014.

[39] H. R. Park et al., " Nucleus accumbens deep brain stimulation for a patient with self-injurious behavior and autism spectrum disorder: functional and structural changes of the brain: report of a case and review of literature ", Acta Neurochir (Wien), vol. 159, no 1, p. 137-143, janv. 2017.

[40] A. Chaddad, C. Desrosiers, L. Hassan, C. Tanougast, " Hippocampus and amygdala radiomic biomarkers for the study of autism spectrum disorder | BMC Neuroscience | Full Text ", Jul. 2017.

[41] C. Q. Choi, " Corpus callosum ages abnormally in autism | Spectrum | Autism Research News ", April 2015.

APPENDIX A

In this part, all regions that were mentioned in the state of the art and were related to ASD were cited below.

White matter: studies have shown that white matter disease is associated with Autism through some physical and emotional symptoms such as balance problems, falls, depression, and difficulty of multitasking activities such walking and talking[37].

Gray matter: Grey matter is involved in muscle control, and sensory perception such as seeing and hearing, speech, self-control, emotions, memory, and decision-making. Researchers found that children diagnosed with autism have more abnormality in gray matter [38].

Nucleus accumbens: The nucleus Accumbens core is involved in the cognitive processing of motor function related to reinforcing slow-wave sleep to regulate reward-motivated behaviors. Some studies related this subcortical region with ASD [39].

Amygdala: the amygdala is related to emotional learning and behavior. Many studies demonstrate that amygdale texture features can be used to extract biomarkers for the characterization of ASD purposes [40].

Corpus callosum: Corpus Callosum the largest white matter structure in the brain. It is involved in the interhemispheric transfer of information and integrates motor, sensory, and cognitive performances. Many comparative studies show that it develops differently in children with autism [41].

Hippocampal: the two most influential theories for hippocampal function are related to space and memory. It is used by the brain for mapping layouts of the environment [40].

Pallidum: Pallidum is a part of the subcortical nervous circuits involved, in motor skills, and, in particular, in the control of posture. It is also associated to non-motor functions (e.g. cognition, emotions, etc...).

Thalamus: Many previous studies shows that the thalamus play a key role in autism. It may regulate social behavior and it is considered as a relay station that merely passes sensory information to the cerebral cortex.

Putamen: the role the putamen is to regulate movements. It employs GABA, acetylcholine, and encephalin to perform its functions.

Caudate nucleus: the caudate nucleus is the subcortical region that controls learning, specifically the storing and processing of memories. Studies show that Autism causes a different development of ASD.

Brainstem: The brain stem is the part of the brain that connects the cerebrum with the spinal cord. The review of the literature suggests that developmental alterations of the brainstem could have potential cascading effects on cortical and cerebellar formation, ultimately leading to ASD symptoms.

APPENDIX B

- Riemannian geometry

Area: The area of a two-dimensional figure or shape is the quantity that expresses the extent of the figure or shape in the the plane. Here in our work, we used (eq 8) to calculate the whole region area by applying the summation of all tetrahedrons areas.

$$A = \sum \frac{1}{2a} * h \tag{8}$$

Where a is the base and h is the height of the triangle.

Volume: The volume is a closed surface that encloses a certain amount of three-dimensional space. Here in our work, we used (eq 9) to calculate the whole region volume by applying the summation of all tetrahedrons volumes.

$$V = \sum \frac{\sqrt{2}}{12} * a^3 \tag{9}$$

Where a is the triangle base.

Isoperimetric ratio: Iso-ratio depends on the volume and the surface. It is initially the study of the properties of the geometric

shapes of the plane (eq 10).

$$IPR = \frac{A}{V^{\frac{2}{3}}} \quad (10)$$

Where A is the triangle area and V is the Volume.

Convexity ratio of the surface: The convex area of an object is the area of the convex hull that encloses the object (eq 11).

$$CRS = \frac{A}{A(CH)} \quad (11)$$

Where A is the triangle area and A (CH) is the convex hull depending on area.

Convexity ratio of the volume: The convex volume of an object is the volume of the convex hull that encloses the object (eq 12).

$$CRV = \frac{V}{V(CH)} \quad (12)$$

Where V is the triangle volume and V (CH) is the convex hull depending on volume.

Gaussian curvature: The Gaussian curvature is defined at a point of a surface contained in Euclidean space as the product of the two main curvatures (eq 13).

$$K = k_1 k_2 \quad (13)$$

Where $k_1$and k_2 are principal curvatures.

Mean curvature: the mean curvature of a surface is called the mean of the minimum and maximum curvatures (eq 14).

$$H = \frac{1}{2}(k_1 + k_2) \quad (14)$$

Where $k_1$and k_2 are principal curvatures.

- Harlicks texture descriptors

The second standard L2N: The second standard measures the length common to all representations of a vector in an affine space (eq 15).

$$|X| = \sqrt{\sum_{k=1}^{n} |x_k|^2} \quad (15)$$

Where |X|is the vector norm and $|x_k|$ is the complex modulus.

Means: Mean is the small mean values indicating coarse texture having a grain size equal to or larger than the magnitude of the displacement vector (eq 16).

$$Mean = \sum_{i=0}^{N-1} \sum_{j=0}^{N-1} Mc(i,j) \quad (16)$$

Where N is the number of gray levels, Mc is the image matrix.

Contrast: The contrast feature is a measure of the image contrast or the number of local variations present in an image (eq 17).

$$Contrast = \sum_{i=0}^{N-1} \sum_{j=0}^{N-1} (i-j)^2 \, Mc(i,j) \quad (17)$$

Where N is the number of gray levels, Mc is the image matrix

Angular Second Moment: Angular Second Moment and Uniformity, also called Energy, which is a measure of textural Uniformity of an image (eq 18).

$$ASM = \sum_{i=0}^{N-1} \sum_{j=0}^{N-1} Mc(i,j)^2 \quad (18)$$

Where N is the number of gray levels, Mc is the image matrix

Variance: This is the sum of the squares of the differences between the intensity of the central pixel and its neighbors (eq 19).

$$V = \sum_{i=0}^{N-1} \sum_{j=0}^{N-1} (i - mean)^2 \, Mc(i,j) \quad (19)$$

Where N is the number of gray levels, Mc is the image matrix.

Standard deviation: The standard deviation is a measure of the amount of variation or dispersion of a set of values (eq 20).

$$\sigma_I^2 = \sum_{i=0}^{N-1} (i - mean)^2 \sum_{j=0}^{N-1} Mc(i,j) \quad (20)$$

Where N is the number of gray levels, Mc is the image matrix

Correlation: Correlation feature shows the linear dependency of gray level values in the cooccurrence matrix: (eq 21).

$$Corr = \frac{1}{\sigma^2} \sum_{i=0}^{N-1} \sum_{j=0}^{N-1} (i - mean)^2 \, Mc(i,j) \quad (21)$$

Entropy: is a measure of information content. It measures the randomness of intensity distribution and the homogeneity of the histogram (eq 22).

$$Entropy = -\sum_{i=0}^{N-1} \sum_{j=0}^{N-1} Mc\,(i,j) \log Mc(i,j) \quad (22)$$

Where N is the number of gray levels, Mc is the image matrix

APPENDIX C

In our work, we employed an Artificial Neural network for the classification. The parameters of a neural network are typically the coefficients of the model. In this case, these parameters are learned during the training stage. So, the algorithm itself, optimizes these coefficients. However, when training it, there are a number of hyperparameters we needed to set, including Table VII.

TABLE VII. HYPERPARAMETERS

Hyperparameters (this is the case of each region)	
Number of hidden layers:	3
Number of units in the input	45
Number of units in first hidden,	90
Number of units in second hidden,	30
Number of units in third hidden	15
Number of units in output layer	1
Learning rate	0.000001
Activation function for 1,2,3,4	activation=tanh'
Activation function for the final layer	activation='sigmoid
Minibatch size	32
Epochs	800
Loss Function	'mean_squared_error'